Microfluid Nanofluid (2013) 14:225–233
DOI 10.1007/s10404-012-1040-5

RESEARCH PAPER

Molecular dynamics simulations of oscillatory Couette flows with slip boundary conditions

Nikolai V. Priezjev

Received: 22 May 2012 / Accepted: 16 July 2012 / Published online: 9 September 2012

Abstract The effect of interfacial slip on steady-state and time-periodic flows of monatomic liquids is investigated using non-equilibrium molecular dynamics simulations. The fluid phase is confined between atomically smooth rigid walls, and the fluid flows are induced by moving one of the walls. In steady shear flows, the slip length increases almost linearly with shear rate. We found that the velocity profiles in oscillatory flows are well described by the Stokes flow solution with the slip length that depends on the local shear rate. Interestingly, the rate dependence of the slip length obtained in steady shear flows is recovered when the slip length in oscillatory flows is plotted as a function of the local shear rate magnitude. For both types of flows, the friction coefficient at the liquid–solid interface correlates well with the structure of the first fluid layer near the solid wall.

Keywords Molecular dynamics simulation · Liquid flow · Nanofluidics · Slip length

1 Introduction

The rational design of micro- and nanofluidics devices requires an accurate prediction of time-dependent flows at the submicron scales (Karniadakis et al. 2005). It is well recognized that fluid flows in confined systems can be significantly affected by slip boundary conditions. The velocity discontinuity is usually quantified via the slip length, which is defined as an extrapolated distance with respect to the liquid–solid interface to the point where the relative tangential velocity component vanishes. At sufficiently high oscillation frequencies, the fluid slip velocity might not be in phase with the substrate velocity, and, therefore, the slip length in general is a complex number (Willmott and Tallon 2007; Ng and Wang 2011). Oscillatory flows with slip boundary conditions of Newtonian liquids were studied experimentally using quartz crystal microbalance (Ferrante et al. 1994; Ellis and Hayward 2003; Du et al. 2004). Molecular dynamics (MD) simulations are particularly well suited to investigate the effects of materials properties of liquid–solid interfaces on flow boundary conditions (Bocquet and Barrat 2007; Li et al. 2010).

A direct comparison between MD simulations and continuum analysis of steady-state flows over chemically textured (Priezjev et al. 2005; Qian et al. 2005; Priezjev 2011) or periodically corrugated (Priezjev and Troian 2006; Niavarani and Priezjev 2008a) surfaces has indicated that there is an excellent agreement of the velocity profiles and the effective slip lengths when the typical length scale of substrate inhomogeneities is about an order of magnitude larger than the molecular size. In the case of time-dependent flows, the main difficulty in extracting flow properties using MD simulations is that averaging over thermal fluctuations has to be repeated over many cycles, which often requires significant computational recourses. The MD simulations of oscillatory flows of monatomic and polymeric fluids have shown that the velocity profiles with no-slip boundary conditions can be well described by the continuum mechanics (Khare et al. 2001). The flow profiles with a finite slip velocity in oscillatory flows were reported at low fluid densities and weak wall-fluid interactions (Hansen and Ottesen 2006; Hansen et al. 2007). More recently, it was shown that the slip length depends on the

N. V. Priezjev (✉)
Department of Mechanical Engineering,
Michigan State University, East Lansing, MI 48824, USA
e-mail: priezjev@egr.msu.edu

magnitude and gradient of shear rate near the oscillating wall, and the fluid slip velocity lags the wall velocity, thus leading to a hysteresis loop (Thalakkottor and Mohseni 2012). However, the dependence of the slip length on the local shear rate or oscillation frequency and amplitude has not yet been systematically investigated.

Molecular dynamics simulations by Thompson and Troian (1997) have shown that in steady shear flow of Newtonian liquids over atomically smooth crystalline surfaces, the slip length is constant at relatively low shear rates and it increases nonlinearly at higher rates. Later, the nonlinear shear rate dependence of the slip length was repeatedly observed in MD studies (Priezjev and Troian 2004; Yang and Fang 2005; Priezjev 2007a, 2012; Asproulis and Drikakis 2010; Niavarani and Priezjev 2010; Wang and Zhao 2011a; Pahlavan and Freund 2011; Wang and Zhao 2011b; Kannam et al. 2012). It was also found that the slip length varies almost linearly with shear rate when liquid and solid phases form incommensurable structures at the interface and the wall–fluid interaction energy is sufficiently high (Priezjev 2007a, b). More recently, it was demonstrated that the characteristic slip velocity associated with the onset of the nonlinear slip regime correlates well with the diffusion time of fluid monomers over the distance between the nearest minima of the periodic surface potential at equilibrium (Priezjev 2010). One of the motivations of the present study is to examine whether shear rate dependent slip boundary conditions observed in steady-state flows are valid for time-dependent flows.

For steady-state flows, a number of previous MD studies have established a correlation between the degree of slip and fluid structure induced by the periodic surface potential (Thompson and Robbins 1990; Barrat and Bocquet 1999; Priezjev 2007a; Niavarani and Priezjev 2008b; Priezjev 2009, 2010; Zhang et al. 2012). In particular, it was shown that for atomically smooth, weakly attractive surfaces, the friction coefficient at the liquid-solid interface is well described by a function of the product of the main peak in the static structure factor and the contact density, both evaluated in the first fluid layer (Priezjev 2010). However, the situation is less clear for time-dependent flows where the surface-induced fluid structure and boundary slip might have a phase difference (especially at high oscillation frequencies), and the conclusions obtained for steady-state flows might not be valid. In the present study, we performed a comparative analysis of the fluid structure and the friction coefficient for steady-state and time-periodic flows.

In this paper, non-equilibrium steady-state and time-periodic molecular dynamics simulations are performed to investigate Couette flows with slip boundary conditions. First, the rate dependence of the slip length is computed in steady shear flows. Then, the velocity profiles in oscillatory flows are compared with the Stokes flow solutions in a wide range of frequencies. We find that the slip length as a function of the local shear rate estimated at the stationary and oscillating walls is in good agreement with the results obtained for steady flows. We will also show that, for both types of flows, the friction coefficient at the liquid–solid interface correlates well with the structure of the fluid layer in contact with the solid wall.

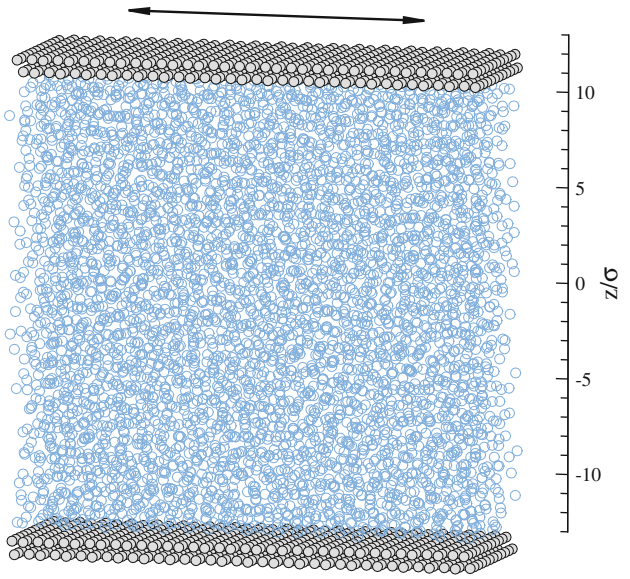

Fig. 1 (Color online) Positions of fluid monomers (*open blue circles*) and wall atoms (*filled gray circles*). The *upper wall* oscillates with the angular frequency ω in the $\hat{x}$ direction (indicated by the *double-sided arrow*), while the *lower wall* is always stationary

The rest of the paper proceeds as follows: In the next section, the details of molecular dynamics simulations are described. In Sect. 3, we briefly review the Stokes flow solution for oscillatory Couette flows, present the results for steady-state shear flows, and then analyze the velocity and density profiles, slip length, and fluid structure in oscillatory flows. Conclusions are given in the last section.

2 Molecular dynamics simulation model

The model system consists of $N_f = 4{,}608$ fluid monomers confined between rigid atomistic walls as shown in Fig. 1. The pairwise interaction between any two fluid monomers is modeled by the Lennard-Jones (LJ) potential

$$V_{LJ}(r) = 4\varepsilon\left[\left(\frac{\sigma}{r}\right)^{12} - \left(\frac{\sigma}{r}\right)^{6}\right], \quad (1)$$

where ε and σ are the energy and length scales, and the cutoff radius $r_c = 2.5\sigma$. In our simulations, the same parameters are used to describe the interaction between fluid monomers and wall atoms; namely, $\varepsilon_{wf} = \varepsilon, \sigma_{wf} = \sigma$, and $r_c = 2.5\sigma$. The wall atoms are fixed rigidly at the lattice sites and do not interact with each other.

The viscous heating generated in the oscillating flow was removed by means of the Langevin thermostat, which was coupled only to the equation of motion perpendicular to the plane of shear as follows:

$$m\ddot{x}_i = -\sum_{i\neq j}\frac{\partial V_{ij}}{\partial x_i}, \tag{2}$$

$$m\ddot{y}_i + m\Gamma\dot{y}_i = -\sum_{i\neq j}\frac{\partial V_{ij}}{\partial y_i} + f_i, \tag{3}$$

$$m\ddot{z}_i = -\sum_{i\neq j}\frac{\partial V_{ij}}{\partial z_i}, \tag{4}$$

where $\Gamma = 1.0\tau^{-1}$ is the friction coefficient and f_i is a random force with zero mean and variance $\langle f_i(0)f_j(t)\rangle = 2mk_{\mathrm{B}}T_{\mathrm{L}}\Gamma\delta(t)\delta_{ij}$ (Thompson and Robbins 1990). In our setup, the temperature of the Langevin thermostat is set $T_{\mathrm{L}} = 1.1\varepsilon/k_{\mathrm{B}}$, where k_{B} is the Boltzmann constant. The equations of motion were integrated numerically using the fifth-order Gear predictor–corrector algorithm (Allen and Tildesley 1987) with a time step $\Delta t = 0.005\tau$, where $\tau = \sqrt{m\sigma^2/\varepsilon}$ is the characteristic LJ time. The length, energy, and time scales for liquid argon are $\sigma = 0.34$ nm, $\varepsilon/k_{\mathrm{B}} = 120$ K, and $\tau = 2.16\times 10^{-12}$ s (Allen and Tildesley 1987).

The fluid phase of density $\rho = 0.81\sigma^{-3}$ is confined between two crystalline walls with density $\rho_{\mathrm{w}} = 2.73\sigma^{-3}$, as illustrated in Fig. 1. Each wall consists of two layers of atoms arranged rigidly on sites of the face-centered cubic (fcc) lattice. The lateral dimensions in the xy plane are measured $L_x = 25.03\sigma$ and $L_y = 9.63\sigma$, and the channel width is fixed $h = 23.58\sigma$. Periodic boundary conditions were applied in the xy plane parallel to the solid walls. This simulation setup is very similar to the one used previously for steady Poiseuille flows (Priezjev 2007a, b), except that in the present study the system size in the $\hat{y}$ direction is slightly larger. In steady shear flows, the fluid viscosity $\mu = (2.15 \pm 0.15)\varepsilon\tau\sigma^{-3}$ was found to be shear rate and temperature independent for $\dot{\gamma}\tau \lesssim 0.072$ and $1.1 \leq Tk_{\mathrm{B}}/\varepsilon \leq 1.35$ (Niavarani and Priezjev 2010).

To simulate the oscillatory Couette flow, the upper wall velocity was varied in the $\hat{x}$ direction with the angular frequency ω and amplitude U, while the lower wall always remained stationary. In the present study, the oscillation frequency was set $\omega\tau = 10^{-1}$, 10^{-2}, 10^{-3}, and 10^{-4} (see Table 1). Before the averaging procedure, the steady-periodic flow was equilibrated during the time interval of about $5\times 10^4\,\tau$. The measurements of the velocity, density, and temperature profiles were made at discrete times $\omega t_n = n\pi/4 + 2\pi m$, where $n = 0, 1, \ldots, 7$ and m is the integer. These profiles were averaged within horizontal bins of thickness $\Delta z = 0.01\sigma$ during the time interval $T/100$, where $T = 2\pi/\omega$ is the period of oscillation. A typical simulation time at low shear rates is about $1.2\times 10^6\tau$.

Table 1 The oscillation frequency ω (in units τ^{-1}), the oscillation period $T = 2\pi/\omega$ (in units τ), the maximum amplitude of the upper wall velocity (in units σ/τ), the upper estimate of the Reynolds number $Re_{\max} = \Delta U h\rho/\mu$, the Stokes boundary layer thickness $\delta = \sqrt{2\,\mu/\rho\,\omega}$ (in units σ), and the corresponding Reynolds number $Re^{\delta}_{max} = \triangle U\delta\rho/\mu$, when $\delta < h = 23.58\sigma$

$\omega\tau$	T/τ	$U_{\max}$	$Re_{\max}$	δ/σ	$Re^{\delta}_{\max}$
0.1	62.83	2.0	6.5	7.29	2.0
0.01	628.32	4.0	18.8	23.04	18.4
0.001	6283.19	6.0	27.6	72.86	–
0.0001	62831.85	6.0	27.6	230.4	–

In the definition of the Reynolds numbers, ΔU is the maximum variation of the tangential fluid velocity component across the channel

3 Results

3.1 Hydrodynamic predictions

The problem of fully-developed oscillatory viscous flow confined between two parallel walls with slip boundary conditions was considered analytically by Khaled and Vafai (2004) and Matthews and Hill (2009). Below, we briefly review the problem and its solution for the flow geometry depicted in Fig. 1. The $\hat{x}$-component of the momentum equation (parallel to the walls) is given by

$$\rho\frac{\partial u_x}{\partial t} = \mu\frac{\partial^2 u_x}{\partial z^2}, \tag{5}$$

where μ and ρ are the fluid viscosity and density. The boundary conditions at the top and bottom walls are specified as follows:

$$z = z_{\mathrm{top}} : u_x = U\sin(\omega t) - L_1\frac{\partial u_x}{\partial z}, \tag{6}$$

$$z = z_{\mathrm{bot}} : u_x = L_2\frac{\partial u_x}{\partial z}, \tag{7}$$

where U is the amplitude and ω is the frequency of oscillation. The slip lengths at the upper and lower walls $L_1 \neq L_2$ are assumed to be constant (Matthews and Hill 2009). We note that the special case $L_1 = L_2$ was considered by Khaled and Vafai (2004).

The solution of the problem Eq. (5) subject to the boundary conditions Eqs. (6, 7) is given by

$$\begin{aligned} u_x(z) = \frac{U}{A^2+B^2}\langle &\exp(+Kz)\times\{[L_2K(A+B)+A]\sin(\omega t+Kz) \\ &+[L_2K(A-B)-B]\cos(\omega t+Kz)\} \\ &+\exp(-Kz)\times\{[L_2K(A+B)-A]\sin(\omega t-Kz) \\ &+[L_2K(A-B)+B]\cos(\omega t-Kz)\}\rangle, \end{aligned} \tag{8}$$

where

$$A = A^+ - A^- \text{ and } B = B^+ + B^-, \tag{9}$$

which in turn are defined as follows:

$$A^{\pm} = \exp(\pm Kh)\{[1 \pm (L_1 + L_2)K]\cos(Kh) - [(L_1 + L_2)K \pm 2L_1L_2K^2]\sin(Kh)\}, \tag{10}$$

$$B^{\pm} = \exp(\pm Kh)\{[1 \pm (L_1 + L_2)K]\sin(Kh) + [(L_1 + L_2)K \pm 2L_1L_2K^2]\cos(Kh)\}, \tag{11}$$

and $K = \sqrt{\omega\rho/2\mu}$. In Sect. 3.3, the velocity profiles obtained from MD simulations will be fitted to Eq. (8) with the parameters L_1 and L_2.

3.2 Steady shear flows

The simulations were first performed at steady-state flow conditions when the upper wall was translated with a constant velocity, while the lower wall always remained stationary. The upper wall velocity was varied in the range $0.025\sigma/\tau \le U \le 6.5\sigma/\tau$. The lower limit was chosen to reduce the averaging time due to thermal fluctuations, while the upper limit was set to avoid the nonlinear slip regime at very high shear rates when the slip velocity becomes much larger than the fluid thermal velocity (Niavarani and Priezjev 2010). In the present study, the maximum slip velocity and shear rate in steady shear flows are about $1.59\sigma/\tau$ and $0.14\tau^{-1}$, respectively, which provide an upper estimate of the Reynolds number $Re \approx 29.5$. It was previously shown for slip flows over periodically corrugated surfaces that the inertia term in the Navier–Stokes equation produces a noticeable difference in the slip length at higher Reynolds numbers of about 130 (Niavarani and Priezjev 2008a).

The representative velocity and density profiles for the upper wall speeds $U = 0.1\sigma/\tau$ and $U = 4.0\sigma/\tau$ are plotted in Fig. 2. As expected, the fluid density profiles exhibit pronounced oscillations near solid walls that gradually decay to the uniform bulk value. The magnitude of the first density peak defines the contact density ρ_c. Notice that the amplitude of the density oscillations is slightly reduced at the higher upper wall speed $U = 4.0\sigma/\tau$. The corresponding velocity profiles, normalized by the upper wall speed, are linear throughout the channel and are characterized by the finite slip velocity at both walls. As clearly observed in Fig. 2b, the relative slip velocity is larger at the higher upper wall speed. Also, it was shown previously for a similar MD setup, that the fluid temperature near the interfaces increases by about 10 % at high shear rates (Priezjev 2007a, b). The correlation between the contact density and fluid temperature in the first layer as a function of the slip velocity was recently reported for polymeric fluids in steady shear flows (Priezjev 2012).

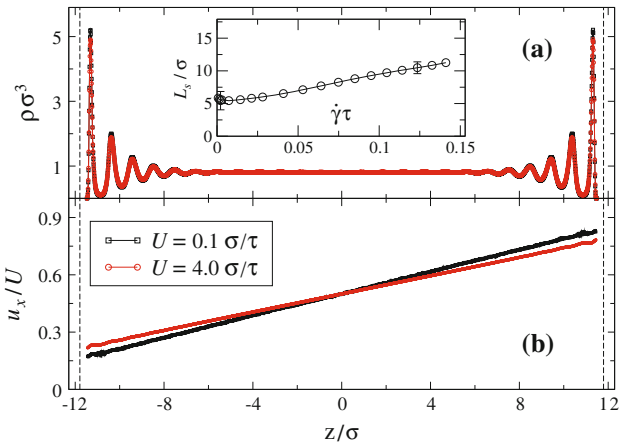

Fig. 2 (Color online) Ensemble-averaged (**a**) density and (**b**) velocity profiles for the indicated upper wall speeds and steady-state flow conditions. The *vertical dashed lines* at $z = \pm 11.79\sigma$ indicate the reference planes for computing the slip length. The *vertical axes* at $z = \pm 12.29\sigma$ coincide with the location of the fcc lattice planes which are in contact with the fluid phase. The *inset* shows the slip length as a function of shear rate when $\omega = 0$

For steady-state flows, the slip length was estimated from the linear extrapolation of the the velocity profiles to $u_x(z) = 0$ below the lower wall and to $u_x(z) = U$ above the upper wall, and then the two values were averaged. The variation of the slip length as a function of shear rate is presented in the inset of Fig. 2a. In agreement with the results of previous studies, where the behavior of the slip length was investigated in a wide range of shear rates and wall–fluid interaction energies (Priezjev 2007a, b), the slip length increases almost linearly with shear rate when $\varepsilon_{wf} = \varepsilon$. It is expected, however, that when the wall-fluid interaction energy is reduced (Priezjev 2007a), then the magnitude of the slip length increases and its shear rate dependence can be well fitted by the power-law function proposed by Thompson and Troian (1997). In the next section, the boundary conditions and fluid structure computed in steady shear flows will be compared with the results obtained for time-periodic flows.

3.3 Oscillatory Couette flows

We next consider oscillatory flows driven by the upper wall, $u_x^w(t) = U\sin(\omega t)$, with frequencies $\omega\tau = 10^{-1}$, 10^{-2}, 10^{-3}, and 10^{-4}. The corresponding period and amplitude of oscillations, the Stokes boundary layer thickness, as well as the upper estimate of the Reynolds numbers are given in Table 1. For each frequency, the amplitude of the velocity oscillation U was chosen such that the fluid slip velocity at the upper wall was always less than $1.5\,\sigma/\tau$. As can be seen from Table 1, the thickness of the Stokes boundary layer is smaller than the channel width

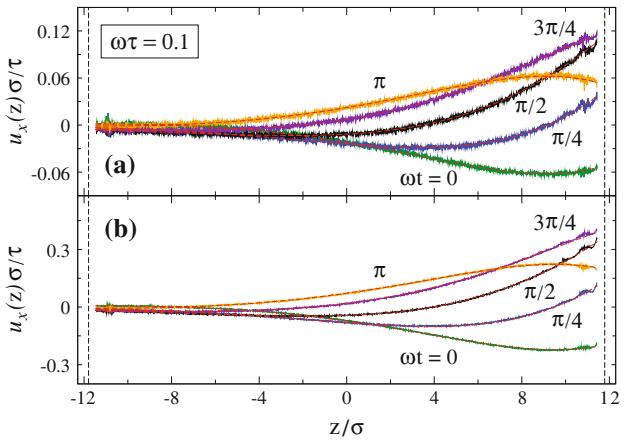

Fig. 3 (Color online) Averaged velocity profiles for oscillatory flows with amplitudes **a** $U = 0.25\sigma/\tau$ and **b** $U = 1.0\sigma/\tau$ and frequency $\omega\tau = 0.1$ at times $\omega t = 0,\ \pi/4,\ \pi/2,\ 3\pi/4$ and π. *The red dashed curves* are the least square fits of Eq. (8) to the MD data. *The vertical dashed lines* at $z = \pm 11.79\sigma$ indicate the reference planes for computing the slip length and shear rate from the best fits to Eq. (8)

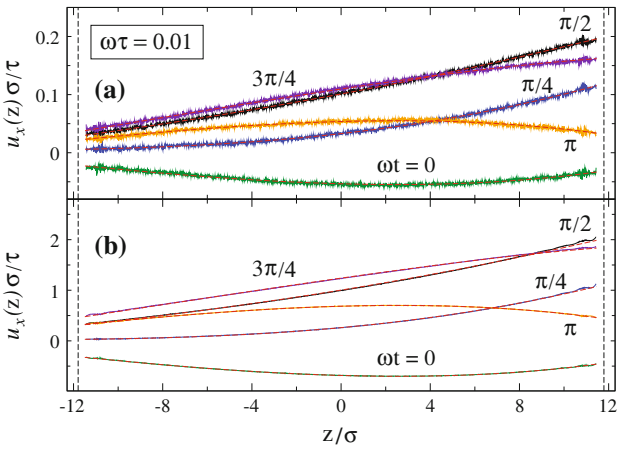

Fig. 4 (Color online) Velocity profiles for time-periodic flows with amplitudes **a** $U = 0.25\sigma/\tau$ and **b** $U = 3.0\sigma/\tau$ and frequency $\omega\tau = 0.01$ at times $\omega t = 0,\ \pi/4,\ \pi/2, 3\ \pi/4$, and π. *The red dashed curves* are the best fits of the MD data using Eq. (8). *The vertical dashed lines* at $z = \pm 11.79\sigma$ denote the location of liquid–solid interfaces

at higher frequencies $\omega\tau = 10^{-1}$ and 10^{-2}. Nevertheless, the upper estimate of the Reynolds number, based either on the channel width or the Stokes layer thickness, is about 27.6, which is indicative of laminar flow conditions. In the present study, the smallest amplitude of the upper wall velocity was set $U = 0.25\sigma/\tau$ in order to compute accurately the velocity profiles without excessive computational efforts.

Examples of the velocity profiles for different frequencies ω and amplitudes U are presented in Figs. 3, 4, 5, 6, and 7. The MD data were averaged over about 20 periods at the lowest frequency $\omega\tau = 10^{-4}$ and over 2×10^4 periods at the highest frequency $\omega\tau = 10^{-1}$. In all figures, the red curves represent the least square fits of the MD data to Eq. (8) with the parameters L_1 and L_2. The shear rate at the upper and lower walls was then computed by taking the derivative of the best fit function $\partial u_x/\partial z$ at $z = \pm 11.79\sigma$. We found that the MD velocity profiles are well described by the continuum solution Eq. (8), except in the interfacial regions of about 2σ at high shear rates. The small discrepancy observed between the MD and continuum results may originate from the inertial effects and/or the fluid temperature increase near the walls at high shear rates.

At the highest frequency $\omega\tau = 0.1$, the Stokes layer thickness is nearly three times smaller than the channel width (see Table 1), and, therefore, the velocity profiles near the stationary lower wall are not significantly affected by the moving upper wall, and, as a result, the interfacial shear rate at the lower wall remains relatively low (see Fig. 3). When $\omega\tau = 0.01$ in Fig. 4, the Stokes layer thickness is approximately equal to the channel width, and the slip velocities and shear rates at the upper and lower walls become comparable. Furthermore, at lower frequencies, $\omega\tau = 10^{-3}$ and 10^{-4}, the flows appear to be quasi-steady and the velocity profiles are nearly linear throughout the channel (see Figs. 6, 7). At the lowest frequency $\omega\tau = 10^{-4}$, the velocity profiles are almost indistinguishable when the magnitude of the upper wall velocity is the same (e.g., when $\omega t = \pi/4$ and $3\pi/4$ in Fig. 7). Notice also that in all cases except $\omega\tau = 10^{-4}$, the velocity profiles at times $\omega t = 0$ and π are symmetrical to each other with respect to the line $u_x = 0$ and the fluid slip velocity is

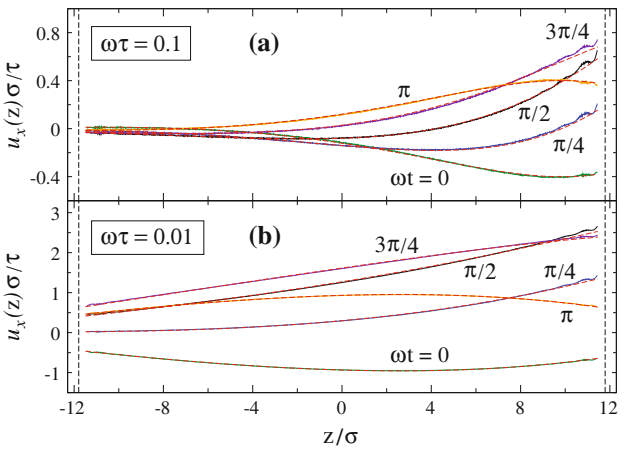

Fig. 5 (Color online) Averaged velocity profiles for **a** $\omega\tau = 0.1$ and $U = 2.0\sigma/\tau$ and **b** $\omega\tau = 0.01$ and $U = 4.0\sigma/\tau$ at times $\omega t = 0, \pi/4,\ \pi/2,\ 3\pi/4$and π. *The dashed curves* are the best fits of the MD data using Eq. (8). The corresponding slip lengths and shear rate magnitudes at the oscillating upper wall are listed in Table 2

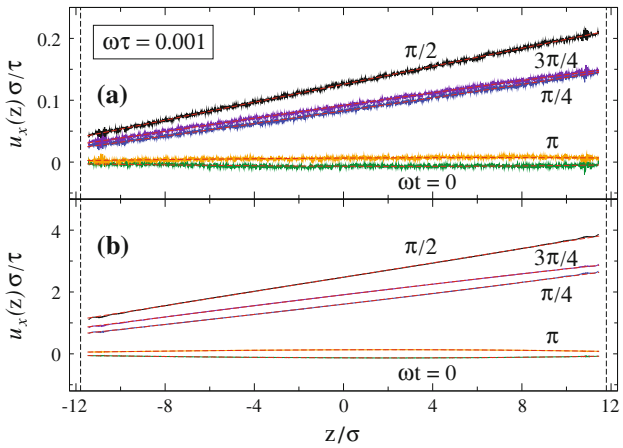

Fig. 6 (Color online) Velocity profiles for oscillatory flows with amplitudes **a** $U = 0.25\sigma/\tau$ and **b** $U = 5.0\sigma/\tau$ and frequency $\omega\tau = 0.001$ at times $\omega t = 0$, $\pi/4$, $\pi/2$, $3\pi/4$, and π. *The dashed curves* represent the best fits of the MD data using Eq. (8). *The vertical axes* at $z = \pm 12.29\sigma$ coincide with the location of the fcc lattice planes

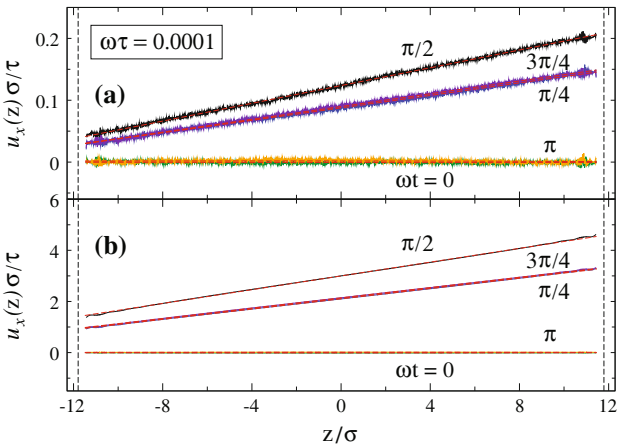

Fig. 7 (Color online) Velocity profiles for time-periodic flows with amplitudes **a** $U = 0.25\,\sigma/\tau$ and **b** $U = 6.0\sigma/\tau$ and frequency $\omega\tau = 0.0001$ at times $\omega t = 0$, $\pi/4$, $\pi/2$, $3\pi/4$, and π. *The red dashed curves* indicate the best fits of the MD data using Eq. (8)

not zero, indicating that the fluid and the upper wall oscillate with the same frequency but with a finite phase difference, which is in agreement with the MD results by Thalakkottor and Mohseni (2012).

The continuum solution for oscillatory slip flows Eq. (8) was derived assuming constant slip lengths at the upper and lower walls. However, when analyzing the velocity profiles computed from MD simulations, we noticed that the fitting parameters L_1 and L_2 in Eq. (8) depend on the interfacial shear rate. The variation of the slip length as a function of the local shear rate computed at the upper and lower walls is plotted in Figs. 8 and 9 for different oscillation frequencies ω, amplitudes U, and times ωt_n. For comparison, the data for steady shear flows are also presented in Figs. 8 and 9 on the log-linear scale to emphasize the low shear rate region. In all cases, the slip length for both oscillatory and steady-state flows is nearly constant at low shear rates $\dot{\gamma}\tau \lesssim 0.01$ and it increases linearly (see inset in Fig. 2) at higher shear rates.

The deviation from the steady-state results in Fig. 8 is most pronounced at the highest frequency $\omega\tau = 0.1$ and the largest amplitude $U = 2.0\sigma/\tau$, when the magnitude of the wall acceleration is maximum, i.e., when $\omega t = 0$ and π (see Table 2; Fig. 5a). Notice also that the MD velocity profiles near the upper wall develop pronounced oscillations at $\omega t = \pi/4$, $\pi/2$, and $3\pi/4$ in Fig. 5a. It can be further observed that, the data in Fig. 8a are scattered at low shear rates because the velocity profiles near the lower wall are not significantly affected by the oscillating upper wall at the highest frequency $\omega\tau = 0.1$ (see Fig. 3), and the statistical errors due to thermal fluctuations become relatively large. Similarly, the averaged fluid velocity is nearly zero when $\omega t = 0$ and π at the lowest frequency $\omega\tau = 10^{-4}$ (see Fig. 7), and, as a result, both L_s and $\dot{\gamma}$ are subject to statistical uncertainty when $\dot{\gamma}\tau \lesssim 0.005$ in Fig. 9b. Remember that, during each cycle, the data were averaged for the time interval $T/100$, and, thus, significantly longer averaging time is required to resolve accurately the velocity profiles in oscillating flows. It is expected, however, that with further averaging, the data in Figs. 8 and 9 for oscillatory flows at low shear rates will converge to the steady-state results.

In the case of slip flow over a planar, impermeable solid surface, the friction coefficient that relates the wall shear stress and slip velocity is equal $k = \mu/L_s$, when the slip length is computed by linear extrapolation of the velocity profile to zero velocity (Willmott and Tallon 2007). However, at higher frequencies, as shown in Fig. 8, the slip lengths L_1 and L_2 computed using Eq. (8) deviate from the slip length in steady-state flows, and, therefore, these values do not provide an accurate estimate of the friction coefficient. Also, the estimate of the interfacial shear rate and the corresponding slip length directly from the MD velocity profiles (e.g., Figs. 3, 4, 5, 6, 7) is not precise because of the slight nonlinearity of the velocity profiles near interfaces and the ambiguity in choosing the size of the fitting region. To avoid the uncertainty associated with fitting the velocity profiles, the friction coefficient in oscillatory flows was estimated from the relation $\sigma_{xz}(t_n) = ku_s(t_n)$. The wall shear stress $\sigma_{xz}(t_n)$ was computed as a ratio of the total tangential force between the fluid monomers and wall atoms to the wall area, and then averaged over the time interval $T/100$. At the same time, the slip velocity was calculated from the velocity and density profiles as follows:

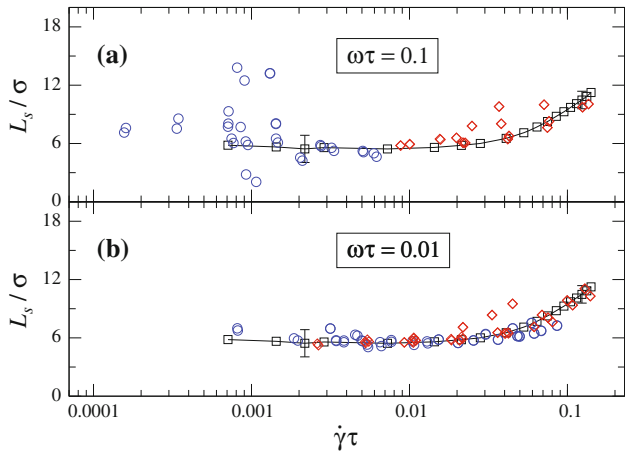

Fig. 8 (Color online) The slip length L_s/σ as a function of shear rate for **a** $\omega\tau = 0.1$ and **b** $\omega\tau = 0.01$. The slip length and the interfacial shear rate are evaluated at the stationary lower wall (*open circle*) and at the oscillating upper wall (*open diamond*). The data for the largest amplitudes U are presented in Table 2. The data for steady shear flows (*open square*) are the same as in the inset of Fig. 2a. *The black curves* are guides to the eye

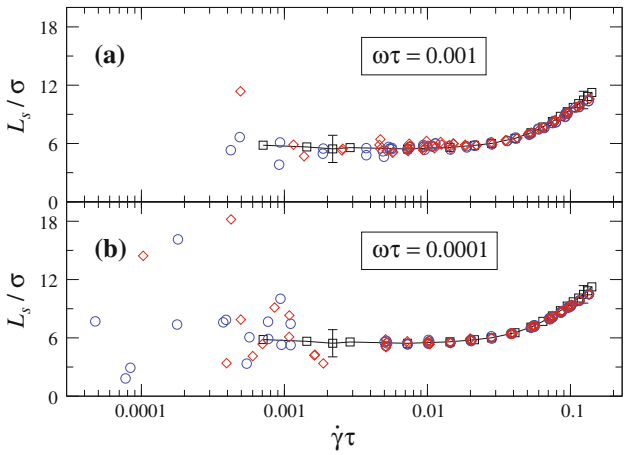

Fig. 9 (Color online) Variation of the slip length as a function of shear rate for **a** $\omega\tau = 0.001$ and **b** $\omega\tau = 0.0001$. The slip length and shear rate are computed at the stationary lower wall (*open cirlce*) and at the oscillating upper wall (*open diamond*). The data (*open square*) are the same as in the inset of Fig. 2a

$$u_s = \int_{z_1}^{z_2} u_x(z)\rho(z)\mathrm{d}z \Big/ \int_{z_1}^{z_2} \rho(z)\mathrm{d}z, \tag{12}$$

where the integrals were taken over the width of the first peaks in the density profiles. Naturally, the fluid slip velocity at the oscillating upper wall is the difference between the velocity of the adjacent fluid layer and the upper wall speed.

As was shown in Fig. 2a, in the presence of a solid substrate, the fluid monomers tend to form several distinct layers that are gradually decaying to a uniform bulk density. In addition to the density layering, the periodic surface potential typically induces an in-plane order within the adjacent fluid layers provided that the wall–fluid interaction energy is sufficiently high (Thompson and Robbins 1990). The characteristic signature of such ordering is the appearance of several sharp peaks in the static structure factor, which is defined as follows:

$$S(\mathbf{k}) = \frac{1}{N_\ell}\left|\sum_{j=1}^{N_\ell} e^{i\mathbf{k}\cdot\mathbf{r_j}}\right|^2, \tag{13}$$

where the sum is taken over N_ℓ fluid monomers in the first layer and $\mathbf{r_j} = (\mathbf{x_j}, \mathbf{y_j})$ is the position vector of the fluid monomer. These peaks are most pronounced at the first reciprocal lattice vectors of the underlying substrate (Thompson and Robbins 1990). Examples of the averaged structure factor and its dependence on the slip velocity were previously reported by Priezjev (2007a) for a similar computational setup. More recently, it was shown for several liquid-on-solid systems that the friction coefficient in steady flows correlates well with the product of the normalized peak in the structure factor and the contact density of the first fluid layer (Priezjev 2010).

In the present study, the friction coefficient in oscillatory and steady-state flows is plotted in Figs. 10 and 11 as a function of the combined variable $S(0)/[S(\mathbf{G_1})\rho_c]$, where $\mathbf{G_1} = (\mathbf{9.04}\sigma^{-1}, \mathbf{0})$ is the first reciprocal lattice vector in the flow direction. For both types of flows, the friction

Table 2 The instantaneous slip lengths and shear rate magnitudes at the oscillating upper wall obtained from the best fit of the MD velocity profiles in Fig. 5 using Eq. (8)

ωt	0	$\pi/4$	$\pi/2$	$3\pi/4$	π	$5\pi/4$	$3\pi/2$	$7\pi/4$
$\omega\tau = 0.1$								
$\dot{\gamma}\tau$	0.037	0.124	0.136	0.071	0.037	0.125	0.136	0.071
L_s/σ	9.8	9.8	10.1	10.0	9.8	9.7	10.1	10.0
$\omega\tau = 0.01$								
$\dot{\gamma}\tau$	0.080	0.140	0.129	0.045	0.080	0.140	0.129	0.045
L_s/σ	7.6	10.3	11.1	9.5	7.6	10.3	11.1	9.5

The amplitude of the upper wall velocity is $U = 2.0\sigma/\tau$ for $\omega\tau = 0.1$ and $U = 4.0\sigma/\tau$ for $\omega\tau = 0.01$. The same data as in Fig. 8

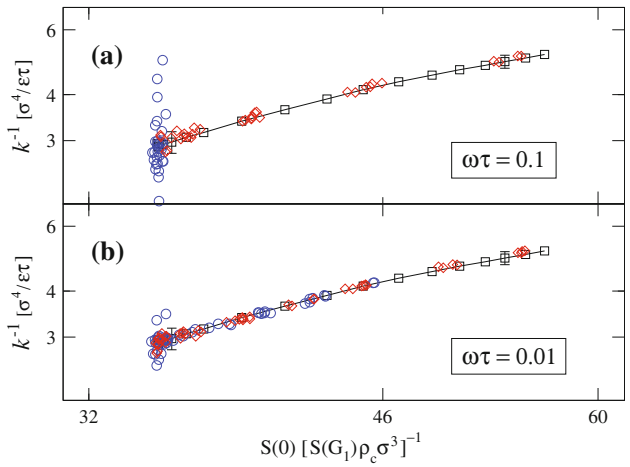

Fig. 10 (Color online) Log–log plot of the inverse friction coefficient as a function of $S(0)/[S(\mathbf{G_1})\rho_c]$ for **a** $\omega\tau = 0.1$ and **b** $\omega\tau = 0.01$. The data for oscillatory flows are denoted by the *red diamonds* (oscillating upper wall) and *blue circles* (stationary lower wall). The data for steady shear flows are indicated by the *black squares*. *The black curves* are guides to the eye

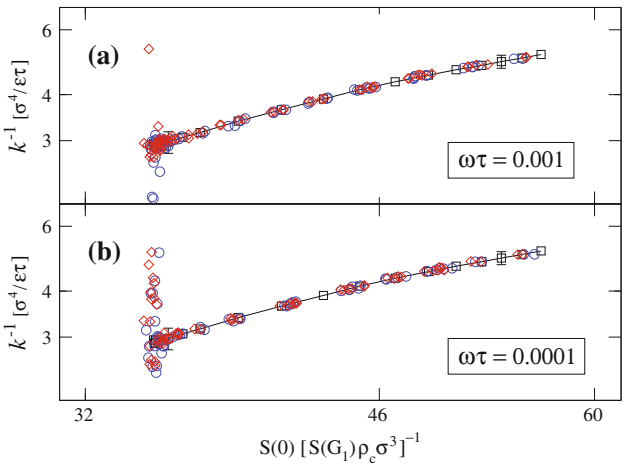

Fig. 11 (Color online) The inverse friction coefficient versus $S(0)/[S(\mathbf{G_1})\rho_c]$ for **a** $\omega\tau = 0.001$ and **b** $\omega\tau = 0.0001$. The friction coefficient and fluid structure are computed at the oscillating upper wall (*open diamond*) and at the lower stationary wall (*open circle*). The data for steady shear flows (*open square*) are the same as in Fig. 10

coefficient and the induced fluid structure are reduced at larger slip velocities. As is evident, the friction coefficient extracted from oscillatory flows agrees well with the the steady-state values, except that the data for periodic flows are scattered as small slip velocities, which is similar to the rate dependence of the slip length reported in Figs. 8 and 9. Interestingly, the agreement at higher frequencies is much better for the friction coefficient (shown in Fig. 10) than for the slip length in Fig. 8. Note also that at the highest frequency $\omega\tau = 0.1$, the period of oscillation $T = 62.83\tau$ is about two orders of magnitude larger than the typical oscillation time of the LJ monomers; but nevertheless, the structure factor and the contact density are nearly the same as in steady-state flows. These results suggest that slip boundary conditions for high-frequency oscillatory flows are more accurately described by the dynamic friction coefficient rather than the slip length as a function of shear rate.

4 Conclusions

In this paper, we have investigated steady and oscillatory Couette flows with slip boundary conditions using molecular dynamics simulations. In both cases, the laminar flows were induced by the moving upper wall while the lower wall remained stationary. The simulations were performed in a wide range of oscillation frequencies; namely, when the Stokes boundary layer thickness is smaller than the channel width at the highest frequency, and, on the other hand, at lower frequencies that correspond to quasi-steady flows. For the chosen parameters, the liquid and solid phases form incommensurate structures at the interface, which is characterized by a finite slip length that increases almost linearly with shear rate.

We found that the velocity profiles computed in MD simulations are well described by the Stokes flow solution with the slip length as a fitting parameter that depends on the local shear rate. The rate dependence of the slip length obtained in steady-state shear flows is reproduced in oscillatory flows when the slip length is measured as a function of the absolute value of the local shear rate. The MD data for oscillatory flows at low shear rates are relatively noisy, which, however, is not surprising given that the velocity profiles were averaged over a small fraction of the period during each cycle. For both types of flows, the friction coefficient at the liquid–solid interface correlates well with the structure factor and the contact density of the first fluid layer.

Acknowledgments Financial support from the National Science Foundation (CBET-1033662) is gratefully acknowledged. Computational work in support of this research was performed at Michigan State University's High Performance Computing Facility.

References

Allen MP, Tildesley DJ (1987) Computer simulation of liquids. Oxford University Press, New York

Asproulis N, Drikakis D (2010) Boundary slip dependency on surface stiffness. Phys Rev E 81:061503

Barrat JL, Bocquet L (1999) Influence of wetting properties on hydrodynamic boundary conditions at a fluid/solid interface. Faraday Discuss 112:119–127

Bocquet L, Barrat JL (2007) Flow boundary conditions from nano- to micro-scales. Soft Matter 3:685–693

Du B, Goubaidoulline I, Johannsmann D (2004) Effects of laterally heterogeneous slip on the resonance properties of quartz crystals immersed in liquids. Langmuir 20:10617–10624

Ellis JS, Hayward GL (2003) Interfacial slip on a transverse-shear mode acoustic wave device. J Appl Phys 94:7856–7867

Ferrante F, Kipling AL, Thompson M (1994) Molecular slip at the solid-liquid interface of an acoustic-wave sensor. J Appl Phys 76:3448–3462

Hansen JS, Ottesen JT (2006) Molecular dynamics simulations of oscillatory flows in microfluidic channels. Microfluid Nanofluid 2:301–307

Hansen JS, Daivis PJ, Todd BD (2007) Local linear viscoelasticity of confined fluids. J Chem Phys 126:144706

Kannam SK, Todd BD, Hansen JS, Daivis PJ (2012) Slip length of water on graphene: Limitations of non-equilibrium molecular dynamics simulations. J Chem Phys 136:024705

Karniadakis GE, Beskok A, Aluru N (2005) Microflows and nanoflows: fundamentals and simulation. Springer, New York

Khaled ARA, Vafai K (2004) The effect of the slip condition on Stokes and Couette flows due to an oscillating wall: exact solutions. Int J Nonlinear Mech 39:795–809

Khare R, de Pablo J, Yethiraj A (2001) Molecular simulation and continuum mechanics investigation of viscoelastic properties of fluids confined to molecularly thin films. J Chem Phys 114:7593–7601

Li Y, Xu J, Li D (2010) Molecular dynamics simulation of nanoscale liquid flows. Microfluid Nanofluid 9:1011–1031

Matthews MT, Hill JM (2009) On three simple experiments to determine slip lengths. Microfluid Nanofluid 6:611–619

Ng CO, Wang CY (2011) Oscillatory flow through a channel with stick-slip walls: complex Navier's slip length. J Fluid Eng 133:014502

Niavarani A, Priezjev NV (2008a) Rheological study of polymer flow past rough surfaces with slip boundary conditions. J Chem Phys 12:144902

Niavarani A, Priezjev NV (2008b) Slip boundary conditions for shear flow of polymer melts past atomically flat surfaces. Phys Rev E 77:041606

Niavarani A, Priezjev NV (2010) Modeling the combined effect of surface roughness and shear rate on slip flow of simple fluids. Phys Rev E 81:011606

Pahlavan AA, Freund JB (2011) Effect of solid properties on slip at a fluid-solid interface. Phys Rev E 83:021602

Priezjev NV (2007a) Rate-dependent slip boundary conditions for simple fluids. Phys Rev E 75:051605

Priezjev NV (2007b) Effect of surface roughness on rate-dependent slip in simple fluids. J Chem Phys 127:144708

Priezjev NV (2009) Shear rate threshold for the boundary slip in dense polymer films. Phys Rev E 80:031608

Priezjev NV (2010) Relationship between induced fluid structure and boundary slip in nanoscale polymer films. Phys Rev E 82:051603

Priezjev NV (2011) Molecular diffusion and slip boundary conditions at smooth surfaces with periodic and random nanoscale textures. J Chem Phys 135:204704

Priezjev NV (2012) Interfacial friction between semiflexible polymers and crystalline surfaces. J Chem Phys 136:224702

Priezjev NV, Troian SM (2004) Molecular origin and dynamic behavior of slip in sheared polymer films. Phys Rev Lett 92:018302

Priezjev NV, Darhuber AA, Troian SM (2005) Slip behavior in liquid films on surfaces of patterned wettability: comparison between continuum and molecular dynamics simulations. Phys Rev E 71:041608

Priezjev NV, Troian SM (2006) Influence of periodic wall roughness on the slip behaviour at liquid/solid interfaces: molecular-scale simulations versus continuum predictions. J Fluid Mech 554:25–46

Qian TZ, Wang XP, Sheng P (2005) Hydrodynamic slip boundary condition at chemically patterned surfaces: a continuum deduction from molecular dynamics. Phys Rev E 72:022501

Thalakkottor JJ, Mohseni K (2012) Analysis of boundary slip in a flow with an oscillating wall. arXiv:1207.7090. http://arxiv.org/abs/1207.7090

Thompson PA, Robbins MO (1990) Shear flow near solids: epitaxial order and flow boundary conditions. Phys Rev A 41:6830–6837

Thompson PA, Troian SM (1997) A general boundary condition for liquid flow at solid surfaces. Nature 389:360–362

Wang FC, Zhao YP (2011a) Slip boundary conditions based on molecular kinetic theory: the critical shear stress and the energy dissipation at the liquid–solid interface. Soft Matter 7:8628–8634

Wang FC, Zhao YP (2011b) The unique properties of the solid-like confined liquid films: a large scale molecular dynamics simulation approach. Acta Mechanica Solida Sinica 24:101–116

Willmott GR, Tallon JL (2007) Measurement of Newtonian fluid slip using a torsional ultrasonic oscillator. Phys Rev E 76:066306

Yang SC, Fang LB (2005) Effect of surface roughness on slip flows in hydrophobic and hydrophilic microchannels by molecular dynamics simulation. Mol Simul 31:971–977

Zhang HW, Zhang ZQ, Ye HF (2012) Molecular dynamics-based prediction of boundary slip of fluids in nanochannels. Microfluid Nanofluid 12:107–115